ChemInform Abstract: Partial Spin Ordering and Complex Magnetic Structure in BaYFeO 4 : A Neutron Diffraction and High Temperature Susceptibility Study.

ARTICLE *in* INORGANIC CHEMISTRY · JANUARY 2014

Impact Factor: 4.76 · DOI: 10.1021/ic4026798 · Source: PubMed

8 AUTHORS, INCLUDING:

Corey M. Thompson
Purdue University
25 PUBLICATIONS **113** CITATIONS

SEE PROFILE

Inorganic Chemistry

Article

pubs.acs.org/IC

Partial Spin Ordering and Complex Magnetic Structure in $BaYFeO_4$: A Neutron Diffraction and High Temperature Susceptibility Study

Corey M. Thompson,*[,†] John E. Greedan,[†] V. Ovidiu Garlea,[‡] Roxana Flacau,[§] Malinda Tan,[∥] Phuong-Hieu T. Nguyen,[∥] Friederike Wrobel,[∥] and Shahab Derakhshan[∥]

[†]Department of Chemistry and Brockhouse Institute of Materials Research, McMaster University, 1280 Main Street W, Hamilton, Ontario L8S 4M1, Canada

[‡]Quantum Condensed Matter Division, Oak Ridge National Laboratory, Oak Ridge, Tennessee 37831, United States

[§]Canadian Neutron Beam Centre, National Research Council, Chalk River Laboratories, Chalk River, Ontario K0J 1J0, Canada

[∥]Department of Chemistry and Biochemistry, California State University Long Beach, 1250 Bellflower Boulevard, Long Beach, California 90840, United States

Supporting Information

ABSTRACT: The novel iron-based compound, $BaYFeO_4$, crystallizes in the *Pnma* space group with two distinct Fe^{3+} sites, that are alternately corner-shared $[FeO_5]^{7-}$ square pyramids and $[FeO_6]^{9-}$ octahedra, forming into $[Fe_4O_{18}]^{24-}$ rings, which propagate as columns along the *b*-axis. A recent report shows two discernible antiferromagnetic (AFM) transitions at 36 and 48 K in the susceptibility, yet heat capacity measurements reveal no magnetic phase transitions at these temperatures. An upturn in the magnetic susceptibility measurements up to 400 K suggests the presence of short-range magnetic behavior at higher temperatures. In this Article, variable-temperature neutron powder diffraction and high-temperature magnetic susceptibility measurements were performed to clarify the magnetic behavior. Neutron powder diffraction confirmed that the two magnetic transitions observed at 36 and 48 K are due to long-range magnetic order. Below 48 K, the magnetic structure was determined as a spin-density wave (SDW) with a propagation vector, $\mathbf{k} = (0, 0, {}^1/_3)$, and the moments along the *b*-axis, whereas the structure becomes an incommensurate cycloid [$\mathbf{k} = (0, 0, \sim 0.35)$] below 36 K with the moments within the *bc*-plane. However, for both cases the ordered moments on Fe^{3+} are only of the order $\sim 3.0\ \mu_B$, smaller than the expected values near $4.5\ \mu_B$, indicating that significant components of the Fe moments remain paramagnetic to the lowest temperature studied, 6 K. Moreover, new high-temperature magnetic susceptibility measurements revealed a peak maximum at ~550 K indicative of short-range spin correlations. It is postulated that most of the magnetic entropy is thus removed at high temperatures which could explain the absence of heat capacity anomalies at the long-range ordering temperatures. Published spin dimer calculations, which appear to suggest a $\mathbf{k} = (0, 0, 0)$ magnetic structure, and allow for neither low dimensionality nor geometric frustration, are inadequate to explain the observed complex magnetic structure.

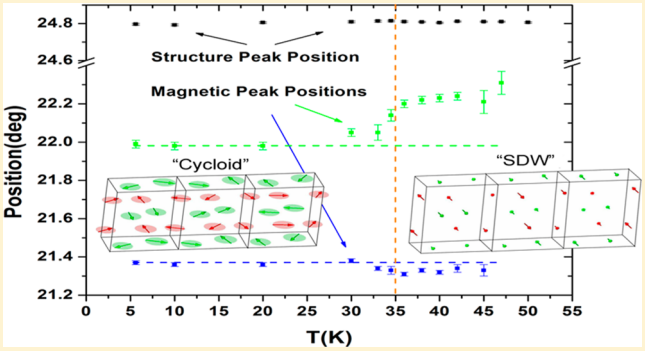

INTRODUCTION

In recent years, various transition metal oxides have been studied for their rich and fascinating properties. Among this class of materials, the Ba−Y−Fe−O system has garnered attention because of $YBa_2Fe_3O_8$, which is analogous to the superconducting cuprate $YBa_2Cu_3O_7$.[1−6] The ability to completely substitute Cu by Fe in $YBa_2Fe_3O_8$ allows for further understanding of structure, superconductivity, and magnetism. Compared to $YBa_2Cu_3O_7$, $YBa_2Fe_3O_8$ is an antiferromagnet at $T_N = \sim 660$ K and has a G-type magnetic structure.

Other materials in the Ba−Y−Fe−O system have been studied due to their unique structural complexity. For instance, Hayward et al. have recently synthesized a number of Ba−Y−Fe−O phases such as Ba_2YFeO_5, $Ba_3YFe_2O_{7.5}$, $Ba_4YFe_3O_{10}$, and $Ba_2YFeO_{5.5}$.[7,8] The latter compound has an Fe^{4+} oxidation state and noncentrosymmetric structure compared to the former compounds which contain Fe^{3+} cations and are complex cation-ordered perovskites. Only $Ba_4YFe_3O_{10}$ and $Ba_2YFeO_{5.5}$ exhibited magnetic ordering and were studied by powder neutron diffraction. $Ba_4YFe_3O_{10}$ appears to be antiferromagnetic below 50 K, and $Ba_2YFeO_{5.5}$ undergoes a magnetic transition at 20 K, which comprises both ferro- and antiferromagnetic ordering.[7,8]

Received: October 24, 2013
Published: January 9, 2014

   dx.doi.org/10.1021/ic4026798 | *Inorg. Chem.* 2014, 53, 1122−1127

Moreover, others have focused on mixed-valent iron oxides because of their rich magnetic properties and charge ordering characteristics, e.g., $YBaFe_2O_5$ and $YBaFe_4O_7$.[9,10] The thermal evolution of $YBaFe_2O_5$ results in three successive classes of mixed valence ($Fe^{2.5+}$) phases that lead to a variety of crystal and magnetic structures. $YBaFe_4O_7$ consists of Fe^{2+}/Fe^{3+} cations and is a spin glass at T_g = 45 K.

In the same vein, to explore further the rich and unique physical properties observed in the Ba−Y−Fe-O system, we have previously synthesized a novel iron-based compound, $BaYFeO_4$,[11] that crystallizes in an orthorhombic *Pnma* space group, isotypic to $Ba_2Y_2CuPtO_8$.[12] There exist two unique Fe^{3+} sites that are alternately corner-shared $[FeO_5]^{7-}$ square pyramids and $[FeO_6]^{9-}$ octahedra, forming into $[Fe_4O_{18}]^{24-}$ rings (Figure 1) which form columns propagating along the *b*-axis, suggesting the possibility of low dimensional magnetism. Our recent study revealed that $BaYFeO_4$ appears to have two distinct, if weak, antiferromagnetic (AFM) transitions at 36 and 48 K in the magnetic susceptibility, but surprisingly, heat capacity measurements showed no magnetic phase transitions at these temperatures. As well, there is an upturn in the magnetic susceptibility data up to 400 K, which suggests the possibility of short-range spin correlations setting in at higher temperatures.

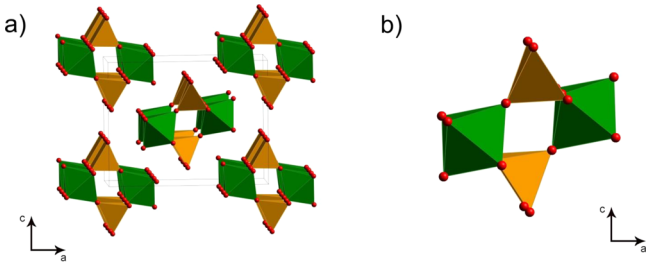

Figure 1. Crystal structure of $BaYFeO_4$. (a) Columns of edge sharing rings $[Fe_4O_{18}]^{24-}$. (b) $[Fe_4O_{18}]^{24-}$ ring formed by corner shared $[FeO_5]^{7-}$ and $[FeO_6]^{9-}$ polyhedra. $[FeO_5]^{7-}$ and $[FeO_6]^{9-}$ polyhedra are shown in gold and green, respectively, and oxygen atoms are red spheres. Barium and yttrium atoms were omitted for clarity.

Clearly, this existing study[11] does not provide a definitive picture of the magnetism in this new iron oxide, and further investigation is warranted. To help clarify the situation we have carried out high-temperature magnetic susceptibility and variable temperature powder neutron diffraction experiments. Herein, we report the results of this investigation including the unusual and complex magnetic structure of this material, an important feature of which is the anomalously small ordered moment on Fe^{3+}.

EXPERIMENTAL SECTION

Synthesis. $BaYFeO_4$ was prepared by a high-temperature ceramic route, as previously reported,[11] but the reaction was scaled up to obtain a sufficient amount of material for neutron diffraction studies (~2 g). Stoichiometric amounts of $BaCO_3$ (99.95%), Y_2O_3 (99.99%; predried at 1000 °C), and Fe_2O_3 (99.99%), were ground together, pressed into pellets, and heated in air for 48 h at 900 °C. The sample was reground and repressed into a pellet and then heated for 48 h at 1250 °C in air. This process was repeated until roughly a phase-pure sample was obtained. Subsequent fitting of the neutron diffraction pattern showed the presence of small amounts of Y_2O_3 (~5%) and $Ba_4Fe_3YO_{10}$ (~8%).

Neutron Diffraction. Powder neutron diffraction measurements were performed on the C2 diffractometer at the Canadian Neutron Beam Centre at Chalk River, Ontario. The data were collected at 14 different temperatures from 6 to 280 K. A wavelength of 1.331 Å with 2θ step size of 0.100° was used to collect data within the 2θ range of 36.9° to 116.9°, and a wavelength of 2.369 Å with the same step size was used for data from 2.9° to 83.0°. Measurements were performed on a sample of ~2 g held in a cylindrical vanadium container in a top-loading closed-cycle refrigerator. The crystal and magnetic structures were refined using FullProf.[13] Representational analysis was used to determine the symmetry allowed magnetic structures with the provided crystal structure and the propagation vector of the magnetic ordering. These calculations were carried out using the program SARAh-Representational Analysis.[14]

Magnetic Property Measurements. A Quantum Design MPMS SQUID magnetometer was used to perform bulk magnetization measurements. The magnetic susceptibility measurements from 300 to 650 K were obtained while heating the sample in a furnace using a quartz sample holder, with applied field of 1000 Oe (0.10 T).

RESULTS AND DISCUSSION

Crystal Structure. Rietveld refinement of the powder neutron diffraction data at 280 K confirmed the orthorhombic *Pnma* structure, in accordance with the previously reported X-ray diffraction data.[11] The results pertaining to lattice constants, positional and displacement parameters, and agreement indices are shown in Table 1. Figure 2 shows the results of the refinement at 280 K. Minor impurities were detected and are attributed to Y_2O_3 (~5% in mass) and $Ba_4YFe_3O_{10}$ (~8% in mass).

Table 1. Refined Crystal Structure Parameters of $BaYFeO_4$ from Powder Neutron Diffraction Data at 280 K[a]

space group	*Pnma*					
lattice parameters	a = 13.171(1) Å					
	b = 5.7061(8) Å					
	c = 10.270(1) Å					
agreement factors	(neutron, λ = 1.331 14 Å)			(neutron, λ = 2.369 76 Å)		
	R(wp) = 4.94; R(p) = 2.98			R(wp) = 5.17; R(p) = 3.68		
	R(exp) = 2.17; R(Bragg) = 5.30			R(exp) = 2.98; R(Bragg) = 5.15		
	$R(F)$ = 2.84			$R(F)$ = 4.64		
atom	Wyckoff	x	y	z	SO	Biso(Å^2)
Ba1	4c	0.21(1)	0.25	0.68(2)	1.0	0.1(2)
Ba2	4c	0.42(1)	0.25	0.40(2)	1.0	0.1(2)
Y1	4c	0.414(9)	0.25	0.01(1)	1.0	0.6(2)
Y2	4c	0.145(9)	0.25	0.31(1)	1.0	0.6(2)
Fe1	4c	0.470(9)	0.25	0.715(9)	1.0	0.3(1)
Fe2	4c	0.188(8)	0.25	0.023(8)	1.0	0.3(1)
O1	4c	0.59(1)	0.25	0.62(2)	1.0	0.8(3)
O2	4c	0.29(1)	0.25	0.18(2)	1.0	0.9(3)
O3	8d	0.006(8)	0.51(2)	0.359(9)	1.0	0.5(2)
O4	8d	0.218(7)	0.51(2)	0.44(1)	1.0	0.6(2)
O5	8d	0.111(8)	1.00(3)	0.13(1)	1.0	0.6(2)

[a]The neutron refinements were done simultaneously with data for two wavelengths.

$BaYFeO_4$ consists of corner shared square pyramids $[FeO_5]^{7-}$ and octahedra $[FeO_6]^{9-}$ which form $[Fe_4O_{18}]^{24-}$ rings. Columns parallel to the *b*-axis are formed via edge sharing of the $[Fe_4O_{18}]^{24-}$ rings, and no atoms fill the voids within these columns (Figure 1).

Variable Temperature Neutron Diffraction. *Neutron Diffraction at T = 6 K.* Figure 3 shows the 50 and 6 K neutron

dx.doi.org/10.1021/ic4026798 | Inorg. Chem. 2014, 53, 1122−1127

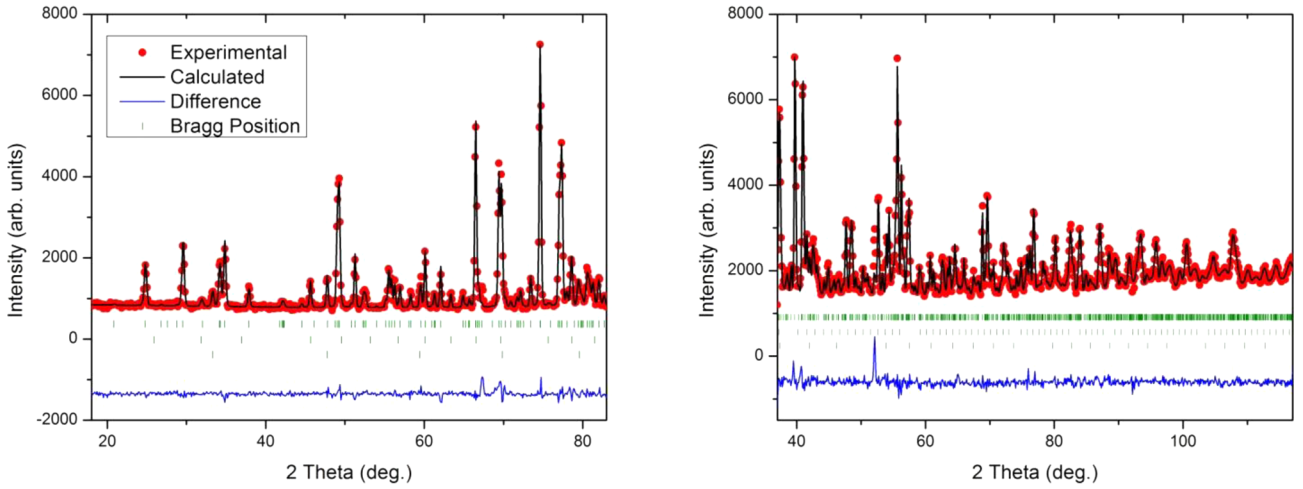

Figure 2. Powder neutron diffraction patterns of $BaYFeO_4$ at 280 K. The diffraction patterns measured at 2.369 Å (left) and 1.331 Å (right). Tick marks represent $BaYFeO_4$, Y_2O_3, $Ba_4YFe_3O_{10}$, respectively. The peak at 51° (right) corresponds to the vanadium sample holder.

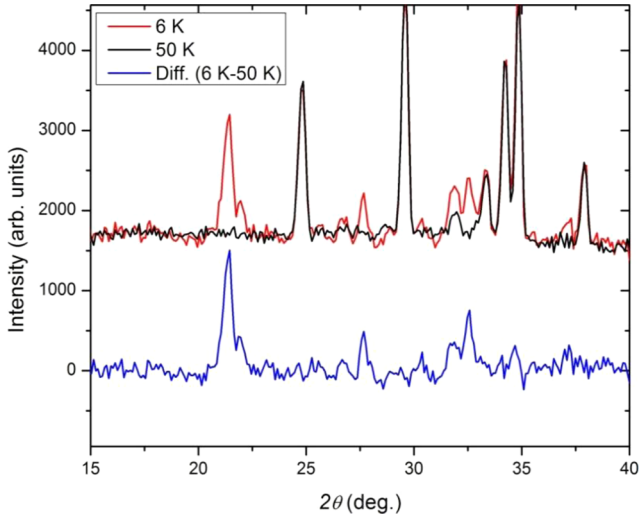

Figure 3. Neutron diffraction patterns at 50 and 6 K, along with the difference between the two patterns.

diffraction patterns along with the difference intensity. There is clear evidence of magnetic peaks at low temperatures which can be indexed with a propagation vector **k** = (0, 0, 0.358(2)), indicating an incommensurate antiferromagnetic structure. In order to determine the possible magnetic structures suitable for the space group *Pnma*, the program SARAh was implemented for representational analysis.[14] The representational analysis resulted in four possible irreducible representations (IRs), Γ_1, Γ_2, Γ_3, and Γ_4 (in Kovalev's notation)[15] provided in Table S1 (Supporting Information). Each of the nonequivalent Fe^{3+} ions ($Fe1,2_{(sp)}$ and $Fe3,4_{(oct)}$) were split into two orbits (sets of magnetically nonequivalent sites). The IRs Γ_1 and Γ_4 describe the magnetic spins arranging along the *b*-axis, whereas Γ_2 and Γ_3 correspond to the spins aligning in the *ac*-plane. The neutron diffraction pattern can be refined using either a spin density wave (SDW) with $M_{Fe}//b$, or a "circular" cycloid magnetic structure lying in the *bc*-plane. The cycloid model has been obtained by combining the basis vectors (BVs) of Γ_4 (spin//*b*) with Γ_2 (spin component//*c*). In both cases (SDW and cycloid), the moments of the structurally equivalent magnetic ions were constrained to be the same $Fe1,2_{(sp)}$ and $Fe3,4_{(oct)}$ and a magnetic phase factor was applied. As indicated in Table 2, the cycloid magnetic model gives a significant improvement in the *R*-factor as compared to the SDW model,

Table 2. Results of the Various Magnetic Structure Refinements at 6 and 38 K for $BaYFeO_4$

param	6 K	38 K
Cycloid		
k-vector	0.358(2)	
magnetic phase (2π) corresponding to $Fe_{(1-4)}$	0; −0.00(2); −0.2(2); 0.2(2)	
$\mu_{Fe1,2}$ (μ_B)	3.0(1)	
$\mu_{Fe3,4}$ (μ_B)	−2.8(1)	
R(Bragg); *R*(F)	12.8; 9.01	
R(Mag)	17.5	
R(p); *R*(wp); *R*(exp)	5.32; 7.08; 3.05	
SDW		
k-vector	0.361(2)	0.3333
magnetic phase (2π) corresponding to $Fe_{(1-4)}$	0; 0.04(2); 0; 0.32(4)	0; 0.03(4); 0; 0.29(6)
$\mu_{Fe1,2}$ (μ_B)	4.4(2)	2.2(2)
$\mu_{Fe3,4}$ (μ_B)	−4.4(2)	−3.0(2)
R(Bragg); *R*(F)	12.7; 8.98	7.20; 5.80
R(Mag)	37.3	36.0
R(p); *R*(wp); *R*(exp)	5.61; 7.35; 3.05	3.59; 4.92; 1.76

and a direct comparison of the calculated intensities to the experimental data also suggests that the 6 K data is described best by the cycloid model (Supporting Information Figure S1). Hence, the cycloid structure was determined as the correct magnetic structure at 6 K (Figure 4). Figure 5 shows the refinement of the cycloid magnetic structure to the 6 K neutron pattern. The refined magnetic moments are 3.0(1) μ_B for Fe1,2 (sp) and −2.8(1) μ_B for Fe3,4 (oct). Furthermore, an elliptical magnetic structure was considered, where the real (*b*-component) and imaginary (*c*-component) parts of the cycloid were unconstrained separately; however, this leads to very similar refinement values to that of the circular cycloid model.

Note, quite remarkably, that the ordered moments on Fe^{3+} are much smaller than those expected for an $S = {}^5/_2$ ion, i.e., between 4.0 and 4.5 μ_B. This indicates that a large component of the Fe^{3+} moment remains disordered, or paramagnetic, down to the lowest temperature studied here, 6 K. This is consistent

dx.doi.org/10.1021/ic4026798 | Inorg. Chem. 2014, 53, 1122−1127

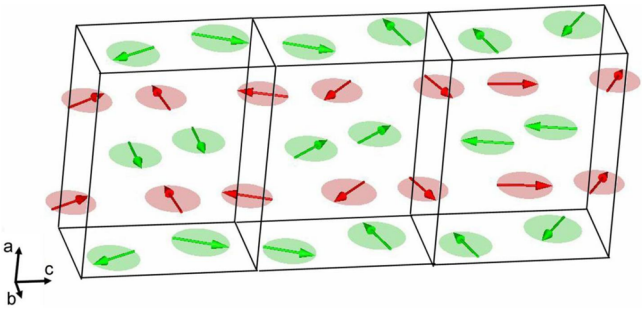

Figure 4. Cycloid magnetic structure at 6 K. The green and red arrows represent the magnetic moments on the square pyramidal and octahedral Fe^{3+} sites, respectively.

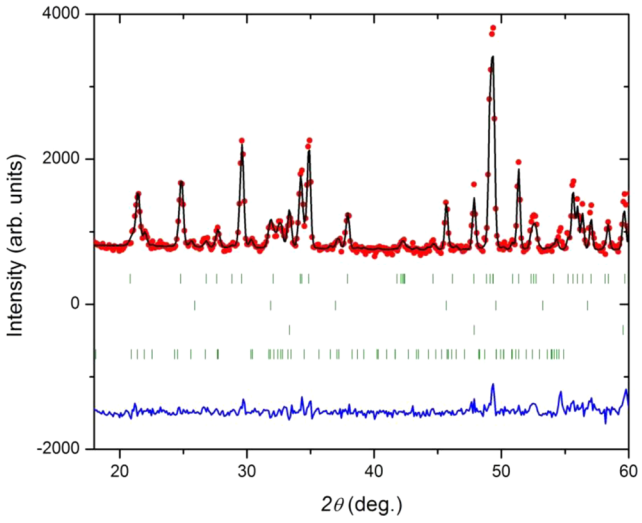

Figure 5. Refinement of the neutron diffraction pattern at 6 K using the cycloid magnetic structure ($\mathbf{k}$ = (0, 0, ~0.35)).

with the large paramagnetic tail observed in the susceptibility data (Figure 10).

Neutron Diffraction at T = 38 K. Figure 6 shows the temperature variation of selected magnetic peaks, showing the onset of magnetic ordering below 50 K, which is in good agreement with previously reported values from magnetic susceptibility measurements.[11] Interestingly, there is evidence of a change in the magnetic structure at around 35 K, as shown from the kinks in the intensity variations. Figure 7 shows the

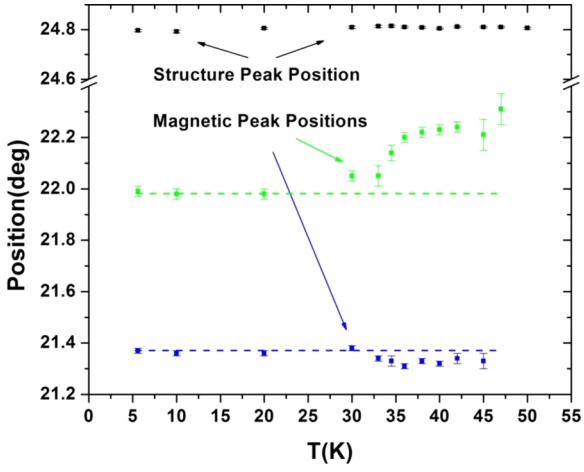

Figure 7. Temperature dependence of selected structural and magnetic peaks positional shifts.

temperature dependence of positional shifts of selected magnetic peaks, which emphasizes the change in the magnetic structure around 35 K compared to the single structural peak which remains invariant with temperature.

The neutron diffraction pattern at 38 K shows the appearance of additional diffraction peaks compared to the 50 K pattern, which can be indexed with a commensurate propagation vector $\mathbf{k}$ = (0, 0, $^1/_3$). In contrast to the neutron pattern refinement at 6 K, the refinement of the 38 K pattern can be undertaken using a spin density wave magnetic structure and sign alternation consistent with Γ_4. In accordance with Landau theory of a second-order phase transition, the magnetic structure has been defined on the basis vectors of only one irreducible representation (Γ_4). Adding an additional spin component belonging to Γ_2, to describe the magnetic phase as a cycloid, does not result in an improved *R*-factor. Similarly to the 6 K refinement, the magnetic moments of the structurally equivalent Fe^{3+} ions were constrained to be the same, but a

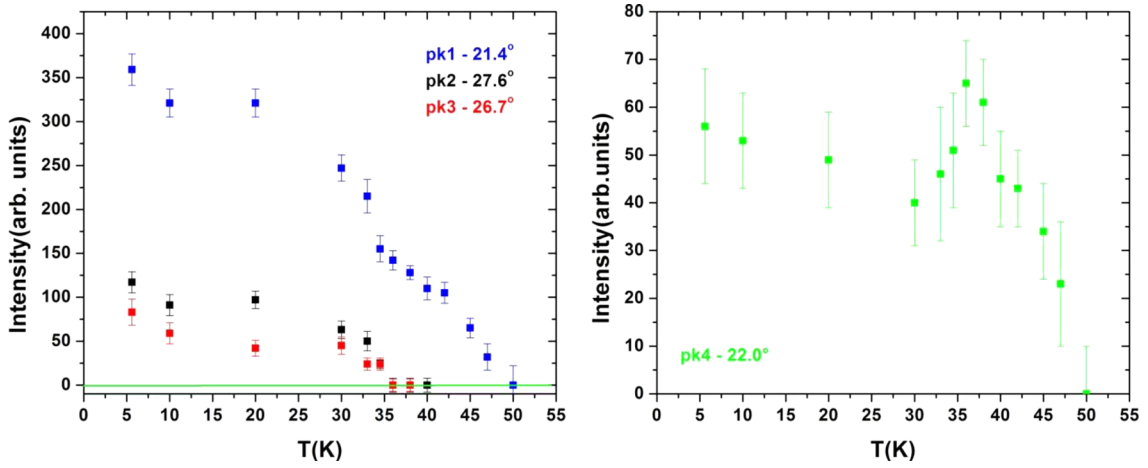

Figure 6. Temperature dependence of the intensities of selected magnetic diffraction peaks. Note: Above 36 K, peaks 1, 2, 3, and 4 correspond to (2 0 $^1/_3$), (2 0 $^4/_3$), (1 1 $^1/_3$), and (0 0 $^5/_3$), respectively. Below 36 K, due to the change in the magnetic structure the peaks 1, 2, 3, and 4 correspond to (2 0 −0.35), (2 0 −1.35), (1 1 −0.35), and (0 0 −1.65), respectively.

dx.doi.org/10.1021/ic4026798 | Inorg. Chem. 2014, 53, 1122−1127

magnetic phase factor was included between magnetically nonequivalent sites (see Table 2). It is noteworthy that the residual factor (*R*-factor) for the magnetic phase is rather high, because the intensities of the magnetic reflections are relatively low. Figure 8 shows the refinement of the spin density wave

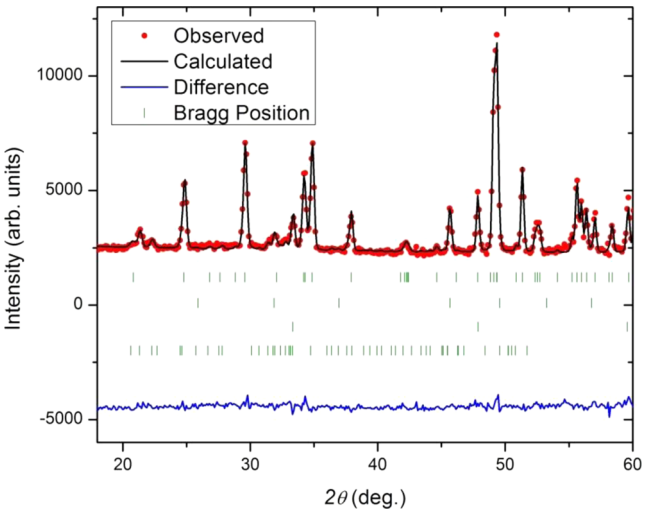

Figure 8. Refinement of the neutron diffraction pattern at 38 K using the spin density wave magnetic structure ($\mathbf{k}$ = (0, 0, $^1/_3$)).

magnetic structure at 38 K. For the SDW magnetic structure, the magnetic moments are oriented along the *b*-axis (Figure 9).

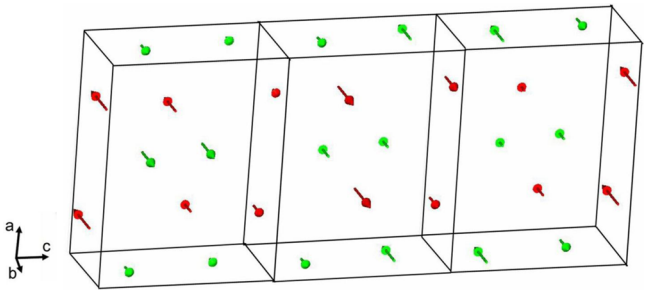

Figure 9. Spin density wave magnetic structure at 38 K. The red and green arrows represent the magnetic moments on the octahedral and square pyramidal Fe^{3+} sites, respectively.

The magnetic moments on the Fe sites are 2.2(2) μ_B for Fe1,2 (sp) and −3.0(2) μ_B for Fe3,4 (oct). Again, these are smaller than expected, indicating a large disordered component to the Fe^{3+} moment.

High-Temperature Magnetic Properties. Figure 10 shows the temperature dependencies of the magnetic susceptibility of $BaYFeO_4$ under applied field of 0.10 T, upon zero-field cooled (ZFC) and field cooled (FC) conditions. The ZFC-FC curves show a slight divergence around ∼200 K. There are clearly two AFM transitions at 36 and 48 K, which agree well with the literature reported values.[11] Fitting the magnetic data to a Curie−Weiss function was unsuccessful, and the previously reported data suggested an upturn in the magnetic susceptibility up to 400 K. This motivated us to measure the sample at higher temperatures. Indeed, there is a broad maximum centered at ∼550 K. This can be taken as evidence for strong short-range spin correlations in this material.

Comparison with Previous Spin-Dimer Calculations. In $BaYFeO_4$, the principal Fe−Fe magnetic interactions are shown in Figure 11 along with the results of a spin dimer

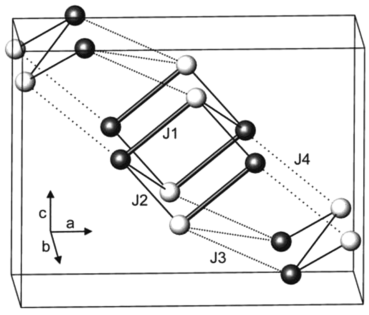

	$\langle(\Delta e)^2\rangle$ [meV^2]	Rel.
J_1	21108	1
J_2	14546	0.69
J_3	8823	0.42
J_4	8678	0.41

Figure 11. Intra- and intercolumn exchange pathways of the Fe−Fe sublattice, J_1−J_4, calculated from a spin dimer analysis.[11] The light and dark spheres correspond to Fe^{3+} square pyramidal and octahedral coordinated environments, respectively.

analysis from the earlier report.[11] All are antiferromagnetic, and while the intracolumn interactions J_1 and J_2 are stronger, the intercolumn exchanges J_3 and J_4 are of the same order of magnitude. Thus, a low dimensional model for the short-range spin correlations seen in the susceptibility is difficult to sustain. As well, the most likely magnetic structure expected from these *J* values would be a simple $\mathbf{k}$ = (0, 0, 0) type pictured in Figure

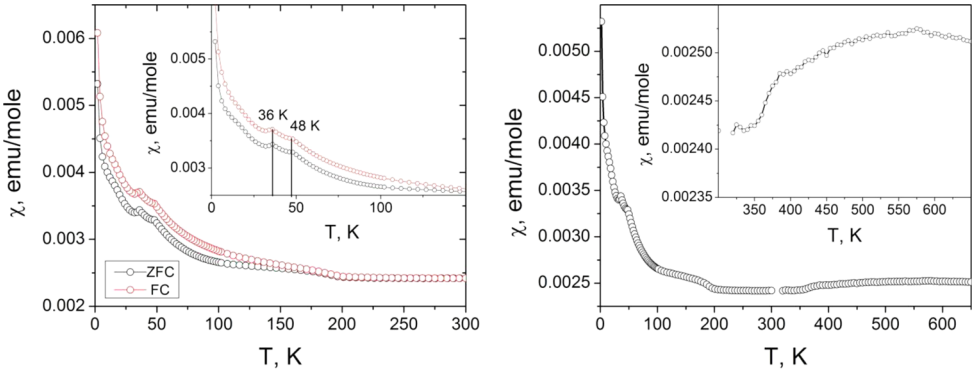

Figure 10. Temperature dependencies of magnetization of $BaYFeO_4$ measured in an applied field of 0.10 T upon ZFC and FC, below 300 K. The inset is the region of the two AFM transitions at low temperature (left). Temperature dependence of magnetization at a longer (higher) temperature range (ZFC). The inset is the region of the high-temperature AFM transition (right).

dx.doi.org/10.1021/ic4026798 | *Inorg. Chem.* 2014, 53, 1122−1127

12. One can expect that this system likely has competing exchange interactions that can lead to magnetic frustration,

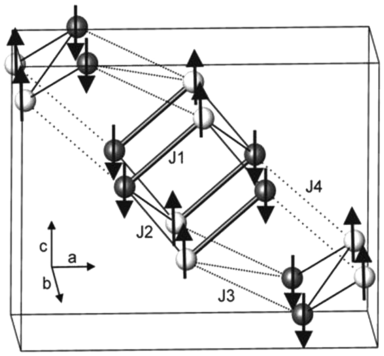

Figure 12. Most likely magnetic structure for $BaYFeO_4$ from the spin dimer results.

competing ground states, and, as a result, a complex magnetic structure. Thus, it is clear that a more detailed analysis of the spin exchange will be needed in order to explain the complex magnetic structure of this remarkable material.

CONCLUSIONS

Variable temperature powder neutron diffraction and high temperature magnetic susceptibility measurements have clarified the magnetic properties of $BaYFeO_4$. The two very weak susceptibility anomalies at 36 and 48 K are identified with the onset of long-range magnetic order but of a very complex type. Below 48 K, the magnetic structure corresponds to a spin density wave with a propagation vector $\mathbf{k} = (0, 0, {}^1/_3)$ with the magnetic moments aligned along the *b*-axis. This transforms below 36 K to an incommensurate structure with propagation vector $\mathbf{k} = (0, 0, \sim 0.35)$ which can be described either by a spin density wave or a cycloid model. Rietveld refinements favor the cycloid structure with Fe^{3+} magnetic moments oriented within the *bc*-plane. A remarkable feature of both magnetic structures is the small ordered moment on Fe^{3+}, $\sim 3.0\ \mu_B$, indicating that a significant fraction of the moment remains paramagnetic down to 5.6 K. This is consistent with the very large paramagnetic tail seen to 2 K in the susceptibility data. As well, high temperature magnetic susceptibility measurements indicate a broad maximum near 550 K indicative of short-range spin correlations. Spin dimer calculations performed previously do not aid in the understanding of the origin of the short-range spin correlations or the complex magnetic structure in this remarkable new iron oxide.

ASSOCIATED CONTENT

Supporting Information

Irreducible representations and basis vectors table, and a figure depicting the refinement comparison of SDW and cycloid magnetic structures at 6 and 38 K. This material is available free of charge via the Internet at http://pubs.acs.org.

AUTHOR INFORMATION

Corresponding Author

*E-mail: thompco@mcmaster.ca.

Notes

The authors declare no competing financial interest.

ACKNOWLEDGMENTS

J.E.G. acknowledges the support of the Natural Sciences and Engineering Research Council (NSERC) of Canada in the form of a Discovery Grant. V.O.G acknowledges the support by the U.S. DOE, Office of Basic Energy Sciences, Scientific User Facilities Division. S.D. is grateful for financial support from the U.S. Army Research Office under Contract/Grant W911NF1210076 and the Research Corporation for Science Advancement (Cottrell College Science Award #19761). We thank Dr. Paul Dube for assistance in collecting the high temperature magnetic susceptibility data.

REFERENCES

(1) Kudryavtsev, D. A.; Mill, B. V.; Vedernikov, N. F.; Shaplygin, I. S. *Inorg. Mater.* **1992**, *28*, 943−946.
(2) Karen, P.; Kjekshus, A.; Huang, Q.; Lynn, J. W.; Rosov, N.; Sora, I. N.; Karen, V. L.; Mighell, A. D.; Santoro, A. P. *J. Solid State Chem.* **1998**, *136*, 21−33.
(3) Huang, Q.; Karen, P.; Karen, V. L.; Kjekshus, A.; Lynn, J. W.; Mighell, A. D.; Rosov, N.; Santoro, A. *Phys. Rev. B* **1992**, *45*, 9611−9619.
(4) Karen, P.; Suard, E.; Fauth, F. *Inorg. Chem.* **2005**, *44*, 8170−8172.
(5) Karen, P.; Kjekshus, A.; Huang, Q.; Karen, V. L.; Lynn, J. W.; Rosov, N.; Natali Sora, I.; Santoro, A. *J. Solid State Chem.* **2003**, *174*, 87−95.
(6) Wu, M. K.; Ashburn, J. R.; Torng, C. J.; Hor, P. H.; Meng, R. L.; Gao, L.; Huang, Z. J.; Wang, Y. Q.; Chu, C. W. *Phys. Rev. Lett.* **1987**, *58*, 908−910.
(7) Luo, K.; Hayward, M. A. *Inorg. Chem.* **2012**, *51*, 12281−12287.
(8) Luo, K.; Johnson, R. D.; Tran, T. T.; Halasyamani, P. S.; Radaelli, P. G.; Hayward, M. A. *Chem. Mater.* **2013**, *25*, 1800−1808.
(9) Woodward, P. M.; Karen, P. *Inorg. Chem.* **2003**, *42*, 1121−1129.
(10) Caignaert, V.; Abakumov, A. M.; Pelloquin, D.; Pralong, V.; Maignan, A.; Van Tendeloo, G.; Raveau, B. *Chem. Mater.* **2009**, *21*, 1116−1122.
(11) Wrobel, F.; Kemei, M. C.; Derakhshan, S. *Inorg. Chem.* **2013**, *52*, 2671−2677.
(12) Swinnea, J. S.; Steinfink, H. *Acta Crystallogr., Sect. C* **1987**, *43*, 2436−2437.
(13) Carvajal-Rodríguez, J. *Physica B* **1993**, *192*, 55−69.
(14) Wills, A. S. *Physica B* **2000**, *276−278*, 680−681.
(15) Kovalev, O. V. *Irreducible Representation of Space Groups*; Gordon and Breach: New York, 1965.